Journal of Catalysis 282 (2011) 258–269

Contents lists available at ScienceDirect

Journal of Catalysis

journal homepage: www.elsevier.com/locate/jcat

Sulfur tolerant metal doped Fe/Ce catalysts for high temperature WGS reaction at low steam to CO ratios – XPS and Mössbauer spectroscopic study

Gunugunuri K. Reddy [a], P. Boolchand [b,*], Panagiotis G. Smirniotis [a,*]

[a] Chemical Engineering Program, School of Energy, Environmental, Biological and Medicinal Engineering, University of Cincinnati, Cincinnati, OH 45221, United States
[b] Department of Electrical and Computer Science Engineering, University of Cincinnati, Cincinnati, OH 45221, United States

ARTICLE INFO

Article history:
Received 13 May 2011
Revised 10 June 2011
Accepted 14 June 2011
Available online 6 August 2011

Keywords:
Modified ferrites
High temperature water gas shift reaction
Mössbauer spectroscopy
TPR
XPS
CeO_2
Magnetite

ABSTRACT

High temperature water gas shift reaction (WGS) at low steam to CO ratios has been investigated over $Fe_{2.4}Ce_{0.3}M_{0.3}O_4$ (M = Cr, Co, Zr, Hf, and Mo) type of spinels in the temperature region of 400–550 °C and in the presence of sulfur. Remarkably, both Cr- and Co-doped Fe/Ce catalysts show excellent activity at steam to CO ratio as low as 1.5. Other dopants namely Zr, Hf and Mo have little or no effect on the WGS activity of Fe/Ce. All the catalysts exhibit excellent stability in the presence of sulfur. X-ray diffraction (XRD) measurements reveal the formation of hematitic phase in *as-prepared* catalysts and magnetite phase in *activated* and *spent* catalysts. After the water gas shift reaction, we observe a decrease in the cell parameter of the magnetite lattice for the *spent* Fe/Ce and Co-, Zr-, Hf-, and Mo-doped Fe/Ce catalysts compared to the activated catalysts. For Cr-doped Fe/Ce catalyst, no change in the lattice parameter was observed after the WGS reaction at a steam/CO ratio = 1.5 and in the presence of sulfur. Temperature-programmed reduction (TPR) measurements suggest that the addition of Zr and Hf to the Fe/Ce lowers the reduction temperature of surface ceria. X-ray photoelectron (XPS) spectra show that both Cr and Co inhibit the carbonate formation in the magnetite during the activation as well as the WGS reaction, whereas Zr, Hf, and Mo can inhibit the formation of carbonate in the magnetite during the activation but not during the WGS reaction. Mössbauer spectral analysis shows that both Cr and Co occupy the octahedral sites of the magnetite during the activation of the catalysts and exhibit higher WGS activity. On the other hand, Zr, Hf, and Mo have little or no effect on the structure and catalytic properties of magnetite either during the activation or during the WGS reaction.

1. Introduction

In recent years, a large number of studies (feasibility, computational, and real time analyses) have been performed on water gas shift (WGS) reaction in membrane reactors [1–6]. The WGS reaction in a membrane reactor (MR) is potentially capable of completing the CO conversion and achieving simultaneous H_2/CO_2 separation in a single stage operation [7,8]. In the MR, the selective permeation of H_2 through the membrane occurs simultaneously as the reaction proceeds and reduces the hydrogen pressure in the catalyst bed to shift the CO conversion (CO) and overcome the equilibrium conversion. By performing WGS reaction in membrane reactors at low steam to CO ratios, one eliminates the thermodynamic limitations and also reduces the operating cost [2,3]. However, problems may arise when using a feed with a low H_2O to CO ratio; side reactions may occur and produce undesired products, such as carbon and/or methane. The formation of carbon could block the catalyst bed and cause catalyst deactivation. The formation of carbon also blocks membrane pores, thus lowering its permeability. For these reasons, it is useful to develop a suitable catalyst for membrane reactor applications that works at low steam to CO ratios.

In our previous study, we developed several transition metal oxide doped iron oxide catalysts with the chemical composition $Fe_{2.73}M_{0.27}O_4$ (M = Cr, Mn, Co, Ni, Cu, Zn, and Ce) for use in membrane reactors for high temperature WGS reaction applications [9,10]. Among the various dopants investigated, Ce-doped iron oxide catalyst exhibited the highest WGS activity at high reaction temperatures ($T > 450$ °C) and higher steam to CO ratios [9]. Ceria (CeO_2) is an oxide with important applications in many areas of chemistry, materials science, and physics [11–13]. In its most stable phase, bulk CeO_2 adopts a fluorite-type crystal structure in which each metal cation is surrounded by eight oxygen atoms [11,14]. Two features are mainly responsible for making cerium a promising material for use either as a support or as a promoter in WGS reactions. These are (a) the redox couple Ce^{3+}/Ce^{4+}, with the ability of ceria to shift between CeO_2 (Ce^{4+}) and Ce_2O_3 (Ce^{3+}) under oxidizing and reducing conditions, respectively, and (b) the ease of formatting of labile oxygen vacancies, and particularly promoting the relatively high mobility of bulk oxygen species [15].

* Corresponding authors. Fax: +1 513 556 3473.
E-mail addresses: boolchp@ucmail.uc.edu (P. Boolchand), panagiotis.smirniotis@uc.edu (P.G. Smirniotis).

0021-9517/$ - see front matter © 2011 Elsevier Inc. All rights reserved.
doi:10.1016/j.jcat.2011.06.016

Cerium oxide-containing WGS catalysts are promising also because of the oxygen storage capacity of ceria and the cooperative effect of Ce-metal in leading to highly active sites [16]. Our previous studies also revealed that both iron and ceria undergo a facile charge transfer reaction between $Fe^{3+} \leftrightarrow Fe^{2+}$ and $Ce^{4+} \leftrightarrow Ce^{2+}$ redox couples, respectively; the synergism between the two couples could be responsible for the improved WGS activity [9]. Additionally, at higher temperatures, the rapid transformation of oxygen exchange between Ce^{3+}/Ce^{4+} redox couple as well as the improvement in the oxygen storage capacity of ceria [17] will help the iron to keep its shift activity high. The problem associated with the Fe/Ce catalyst is that it becomes less active at low steam to CO ratios.

The present study is focused on developing a novel series of sulfur tolerant Fe/Ce catalysts for membrane reactor WGS applications. We focus on operation at low steam to CO ratios, conditions that are of unique industrial interest. For this purpose, various metal (Cr, Co, Mo, Zr, and Mo) doped Fe/Ce catalysts of a fixed doping concentration were prepared by ammonia assisted co-precipitation method. The synthesised catalysts were evaluated for high temperature WGS reaction at steam/CO ratios = 3.5 and 1.5 in a traditional fixed bed reactor. We found that the structural, surface properties, and catalytic performance of metal doped Fe/Ce catalysts depend on the nature of dopant. Remarkably, both the Cr- and Co-doped Fe/Ce catalysts exhibit excellent activity at low steam to CO ratios for the high temperature WGS reaction and reach equilibrium conversions at steam/CO ratio = 1.5. All the catalysts show excellent stability in the presence of 400 ppm of sulfur. No deactivation of any catalyst is observed in the presence of sulfur. Structural characterization measurements show that both Cr and Co dopants act to stabilize the magnetite phase and inhibit the sintering of it during the activation and WGS reaction. However, surface characterization measurements suggest that these dopants hinder the $Fe^{2+} \leftrightarrow Fe^{3+}$ structural rearrangement on the surface of doped magnetite. A plausible explanation for the role of these Cr- and Co-doped ferrites on WGS activity is proposed using local and extended range structural data available from Mössbauer, XRD, and XPS measurements, respectively.

2. Experimental

2.1. Catalyst preparation

Ammonia assisted co-precipitation route is explored for high-yield preparations of various modified spinels Fe/Ce/M (M = Cr, Co, Mo, Zr, and Hf) at atomic ratios 10:1:1. In a typical preparation, calculated amounts of iron nitrate, cerium nitrate, and the corresponding dopant metal nitrate were dissolved separately in deionized water and mixed together. Dilute aqueous ammonia was added gradually dropwise to the aforementioned mixture solutions, with vigorous stirring, until precipitation was complete (pH ≈ 9). The supernatant liquid was analyzed for nitrate ions by adding about 1 ml concentrated sulfuric acid to 10 ml of the supernatant, while the formation of $[Fe(NO)]^{2+}$ can be detected by a brown ring [18]. The formation of brown ring was not observed in all the cases. Thus, the obtained precipitate gels were further aged overnight and filtered off. The obtained cakes were oven dried at 80 °C for 12 h and finally calcined at 500 °C for 3 h in inert environment. The rate of heating as well as cooling was always maintained at 5 °C min^{-1}.

2.2. Catalyst characterization

2.2.1. Surface area and pore size distribution analysis

The BET surface areas were obtained by N_2 adsorption on a Micromeritics 2010 Instrument. Prior to analysis, samples were oven dried at 120 °C for 12 h and flushed with Argon for 3 h. All samples were degassed at 300 °C under vacuum before analysis. The pore size distribution analyses were conducted by N_2 physisorption at liquid N_2 temperature using Micromeritics ASAP 2010 apparatus.

2.2.2. X-ray diffraction measurements

Powder X-ray diffraction (XRD) patterns were recorded on a Phillips Xpert diffractometer using nickel-filtered Cu Kα (0.154056 nm) radiation source. The intensity data were collected over a 2θ range of 3–80° with a 0.02° step size and using a counting time of 1 s per point. Crystalline phases were identified by comparison with the reference data from ICDD files. The average crystallite size was estimated with the help of the Debye–Scherr equation, using the XRD data of all prominent lines [19]. Lattice parameter estimations were carried out by employing standard indexation methods using the intensity of high 2θ peaks (2 1 4) and (3 0 0) [19–21].

2.2.3. TPR measurements

The temperature-programmed reduction (TPR) with hydrogen, of various catalyst samples, was performed by means of an automated catalyst characterization system (Micromeritics, model AutoChem II 2920), which incorporates a thermal conductivity detector (TCD). The experiments were carried out at a heating rate of 5 °C/min. The reactive gas composition was H_2 (10 vol.%) in Argon. The flow rate was fixed at 10 ml/min (STP). The total reactive gas consumption during TPR analysis was measured. The TPR measurements were carried out following activation after cooling the sample in helium flow to 50 °C. The sample was then held at 50 °C under flowing helium to remove the remaining adsorbed oxygen until the TCD signal returned to the baseline. Subsequently, the TPR experiments were performed up to a temperature 800 °C. The water formed during the reduction was removed by using a trapper. The gas stream coming from the reactor was passed through a trapper before the gas entered into the GC. A mixture of isopropanol and liquid nitrogen was used in the trapper to trap the formed water during the TPR experiment.

2.2.4. Mössbauer spectral analysis

^{57}Fe Mössbauer spectra were recorded in a transmission geometry using a constant acceleration spectrometer with liquid helium metal dewar [22]. Experiments were performed at room temperature. A 20 mCi of ^{57}Co (Rh) was used as an emitter, and the spectrometer was calibrated using a α-Fe foil, and taking the isomer shift of Rh at −0.15 mm sec^{-1} w.r.t. α-Fe. Linewidths, on the inner two lines of α-Fe, were typically found to be 0.22 mm/s. An 80 mg quantity of the oxide catalyst as a fine powder was spread on a thin Teflon sheet using GE varnish as a binder and used as an absorber. Typical run lasted 48 h, and base line counts per channel were two millions. Mössbauer spectroscopy of as-prepared, activated, and used catalysts after the WGS reaction was measured. The catalyst was mixed with GE varnish in nitrogen hood to prevent hydrolysis from ambient air.

2.2.5. XPS measurements

The X-ray photoelectron spectroscopy (XPS) measurements were performed on a Pyris VG thermo scientific spectrometer using Al Kα (1486.6 eV) radiation as the excitation source. Charging of the catalyst samples was corrected by setting the binding energy of the adventitious carbon (C 1s) at 284.6 eV. The XPS analysis was performed at ambient temperature and at pressures typically on the order of $<10^{-8}$ Torr. Prior to analysis, the samples were out gassed under vacuum for 4 h. The Fe2p spectra were deconvoluted to find out the ratio between Fe^{2+} and Fe^{3+} on the surface. The details of curve fitting procedure are as follows: (1) select binding energy range for background subtraction; (2) select the linear

method for the background subtraction; (3) select Gaussian-Amplitude for peak selection; (4) select the asymmetry factor as 1; (5) select area for the specific peaks; and (6) select the best fitted curve for experimentally obtained Fe2p, which gives the minimum chi square. These steps were repeated until best chi squared given.

2.3. Catalyst activity

The WGS reaction was carried out in a vertical down flow fixed bed differential ceramic microreactor (i.d. 0.635 cm) at atmospheric pressure. In a typical experiment, ca. 0.1 g of powdered catalyst was placed between two plugs of quartz wool. The reactor was placed vertically inside a programmable tubular furnace (Lindberg), which was heated electrically. The catalyst pre-treatment involves the partial reduction of hematite (Fe_2O_3) to magnetite (Fe_3O_4) using a process gas (mixture of H_2, CO, CO_2, (99.9% pure gases) and water vapor) [23–25] with an reductant to oxidant ratio of $R = 1.4$ ($R = [CO_2] + [H_2O]/[CO] + [H_2]$). Prior to the reaction, the catalyst was pre-treated in flowing process gas at 400 °C for 4 h. It is important to avoid over-reduction of the magnetite active phase to lower carbides, oxides, or metallic iron phases. Metallic iron phases are active catalysts for methanation and Fischer–Tropsch processes [23]. The rate of heating and cooling was always maintained at 5 °C min^{-1}. The gas flows were regulated through pre-calibrated mass flow controllers with digital read-out unit (MKS instruments). Water was injected into the system through a motorized syringe pump (Cole-Parmer type 74,900) to generate steam. The entire system was kept at 200 °C by using heating tapes. Before pre-treatment, the reactor set-up was flushed with an inert gas, and the pre-treatment gas mixture was initialized only after the catalytic system had attained temperatures higher than 150 °C. The experiments were performed in the temperature region of 400–550 °C using a constant steam to CO ratios equal to 1.5 and 3.5. The gas hourly space velocity of 60,000 h^{-1} was maintained in all the experiments. The product stream coming from the reactor was passed through ice cooled trap to condense water, after which the product gases were analyzed with an online TCD (Gow Mac series 550 thermal conductivity detector) having a porapak Q column for separation of the gases. This TCD was interfaced to a personal computer using a peak simple chromatography data system. The postanalyses of results were done on the peak simple 2.31 software. The product-gas was injected through a six port valve, and sampling was performed every 20 min intervals. In this study, the reported values of conversions correspond to steady-state values at 12 h on stream.

3. Results and discussion

Prior to the initial use of the catalysts, iron(III) oxide hematite (Fe_2O_3) is reduced to magnetite (Fe_3O_4) using the reformer product gases, where excess additional steam is introduced to control the proper extent of the reduction [26–28]. Over-reduction of the catalyst to FeO or Fe causes the loss of the active component (Fe_3O_4) as well as physical damage of the catalyst. In such a case, a damaging hot spot can form during the reaction due to exothermic methanation for which metallic iron is known to be a good catalyst [27]. Thus, it is very desirable to avoid over-reduction of the Fe_3O_4 during pre-reduction as well as the WGS reaction [27]. It is generally known from industrial experience that if the reduction factor (R) for the reformed gas is maintained at less than 1.2, then over-reduction of Fe_3O_4 does not occur, while over-reduction consistently occurs when R is greater than 1.6 [24,26]. In the present study, an optimal reduction factor (R) equal to 1.4 was utilized without adding any additional steam.

High temperature WGS reaction has been carried out over the activated Fe/Ce and metal doped Fe/Ce catalysts at steam/CO ratios = 3.5 and 1.5 in the temperature region from 400 to 550 °C. A relatively high space velocity of 60,000 h^{-1} was used in the present study. The WGS reaction conditions were chosen to mimic the membrane reactor applications [29]. The WGS activity profiles of Fe/Ce and various metal doped Fe/Ce catalysts at steam/CO ratio = 3.5 are shown in Fig. 1. The reported conversion values are taken after 12 h of time on stream. In general with increasing temperature, the WGS activity is found to increase. No pressure drop across the catalyst bed is observed during the experiments nor was CH_4 detected in the effluent stream. Interestingly, all the doped and Fe/Ce catalyst reached equilibrium conversions at the highest temperature investigated (550 °C). Among the various dopants, both Cr- and Co-doped Fe/Ce catalysts exhibited high activity at lower reaction temperatures (400–500 °C). The remaining dopants, Zr, Hf, and Mo in Fe/Ce catalysts, had little or no effect on the WGS activity at steam/CO ratio = 3.5. They exhibited the same activity as Fe/Ce. Fig. 2 shows the WGS activity profiles of Fe/Ce and various metal doped Fe/Ce catalysts at steam to CO ratio of 1.5. As expected, by decreasing the steam to CO ratio from 3.5 to 1.5, a decrease in the WGS activity of Fe/Ce, and Zr-, Hf-, and Mo-doped Fe/Ce catalysts was observed. However, both Cr- and Co-doped Fe/Ce catalysts keep their high WGS activity at steam/CO ratio = 1.5. Both Cr- and Co-doped catalysts reached equilibrium conversions at the highest

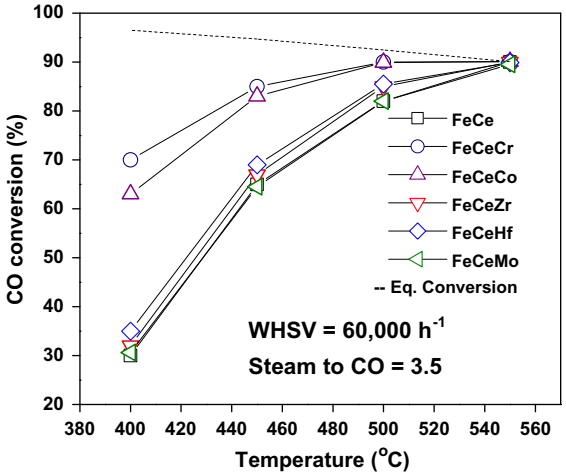

Fig. 1. WGS activity results of Fe/Ce and various Fe/Ce/M (M = Cr, Co, Zr, Hf, and Mo) catalysts (WHSV = 60,000 h^{-1}, Steam to CO ratio = 3.5).

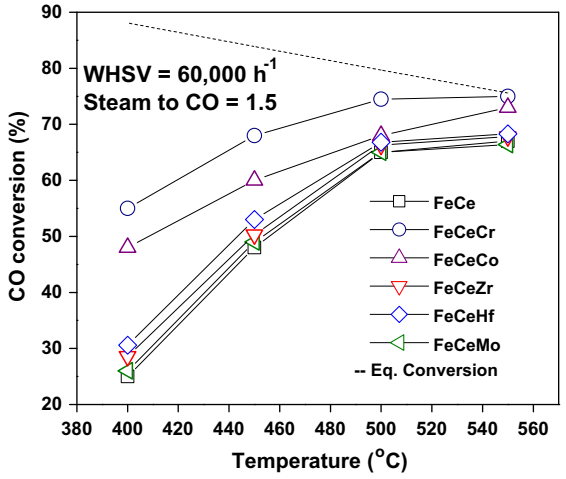

Fig. 2. WGS activity results of Fe/Ce and various Fe/Ce/M (M = Cr, Co, Zr, Hf, and Mo) catalysts (WHSV = 60,000 h^{-1}, Steam to CO ratio = 3.5).

reaction temperature of 550 °C. Between the two dopants, Cr and Co, Cr-doped Fe/Ce catalyst exhibited the highest WGS activity. The activated ferrites were also tested for sulfur tolerance. Fig. 3 presents the WGS activity profiles of Fe/Ce and metal doped Fe/Ce catalysts in the presence of 400 ppm of sulfur at steam/CO ratio = 1.5. Interestingly, none of the catalysts show deactivation in the presence of sulfur. All the catalysts exhibited excellent stability toward 400 ppm of sulfur. In general, in the presence of sulfur, catalysts become sulfided with Fe_3O_4 converting to FeS [30,31]. In the present study, in the presence of sulfur, no formation of FeS was observed from the XPS studies after the WGS reaction. This is probably due to the resistance of ceria toward sulfurization. Ceria stabilizes magnetite from the sulfiding during the WGS reaction. Thus, WGS activity results suggest that both Cr- and Co-doping provide high activity at low steam to CO ratios as well. Other dopants Zr, Hf, and Mo have little or no effect on the WGS activity of Fe/Ce. Ceria stabilizes the magnetite during the WGS reaction in the presence of sulfur.

3.1. Structural and surface properties

To investigate the structural changes during calcination, activation, and the WGS reaction, XRD measurements were performed over *as-prepared*, *activated*, and *spent* catalysts after the WGS reaction at steam to CO ratio of 1.5 and in the presence of sulfur. XRD patterns of *as-prepared* catalysts are presented in Fig. 4. The eight major reflections centered at 21.38°, 25.48°, 30.38°, 35.68°, 43.58°, 53.98°, 57.28°, and 62.78° in the XRD pattern of the fresh Fe/Ce catalyst correspond well to those of α-Fe_2O_3 structure [32]. In addition to these peaks, one more peak was observed at 2θ = 29.2°. This peak is due to the cubic fluorite structure of ceria [33]. Both Cr- and Co-doped Fe/Ce catalysts exhibit completely amorphous patterns. On the other hand, Zr-, Hf-, and Mo-doped Fe/Ce catalysts show intense peaks due to both hematite and ceria in the XRD patterns. In the case of Zr- and Hf-doped Fe/Ce catalysts, the peak due to ceria has been shifted to a higher 2θ value. This is due to the formation of solid solution between Ce and Zr/Hf as reported by several authors [34]. No reflections corresponding to any of the third doped metal oxide, i.e., Cr_2O_3, Co_3O_4, ZrO_2, HfO_2, and MoO_3 or compounds are observed. The activated Fe/Ce catalyst (Fig. 5) exhibited seven reflections in its XRD pattern at 17.38°, 29.88°, 35.58°, 43.18°, 53.48°, 57.08°, and 62.58°, which we identified with those of Fe_3O_4 (magnetite) inverse cubic spinel. Magnetite crystallizes in an AB_2O_4 structure where A represents tetrahedral sites that are occupied by 1/3rd of Fe^{3+} ions and B represents octahedral sites that are occupied by 2/3rd of Fe^{3+} and Fe^{2+} ions. The oxidation–reduction cycle of iron cations is responsible for the catalytic activity. Hence, it is very important to convert hematite to magnetite during the pre-reduction of catalysts without any over-reduction. Interestingly, in the present study, there is no evidence for the formation of Fe (metallic) or FeO phases due to over-reductions, which are inactive phases for the WGS reaction. The XRD results on *spent* catalysts after the WGS reaction (Fig. 6)

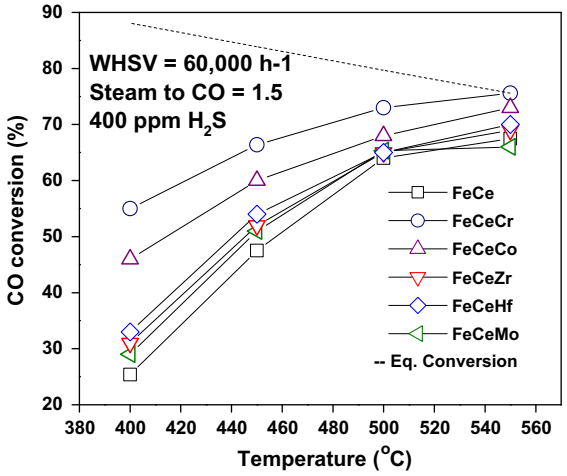

Fig. 3. WGS activity results of Fe/Ce and various Fe/Ce/M (M = Cr, Co, Zr, Hf, and Mo) catalysts (WHSV = 60,000 h^{-1}, Steam to CO ratio = 3.5, 400 ppm H_2S).

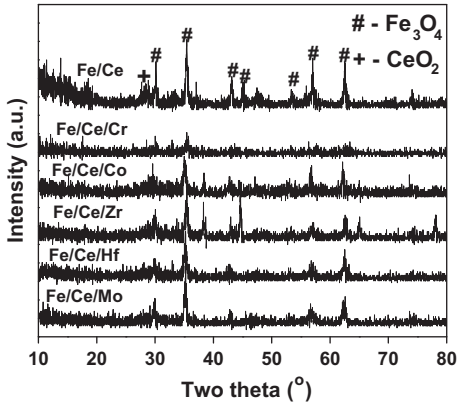

Fig. 5. X-ray powder diffraction patterns of Fe/Ce and various Fe/Ce/M (M = Cr, Co, Zr, Hf, and Mo) activated catalysts (* – Fe_3O_4, + – CeO_2).

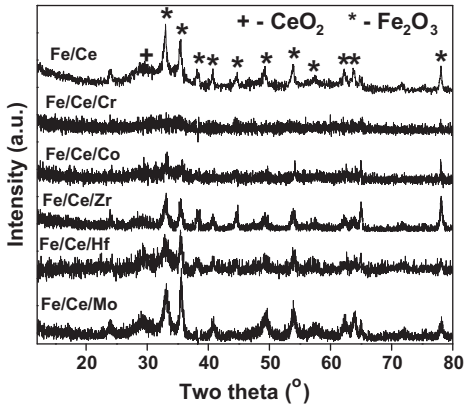

Fig. 4. X-ray powder diffraction patterns of Fe/Ce and various Fe/Ce/M (M = Cr, Co, Zr, Hf, and Mo) fresh catalysts (* – Fe_3O_4, + – CeO_2).

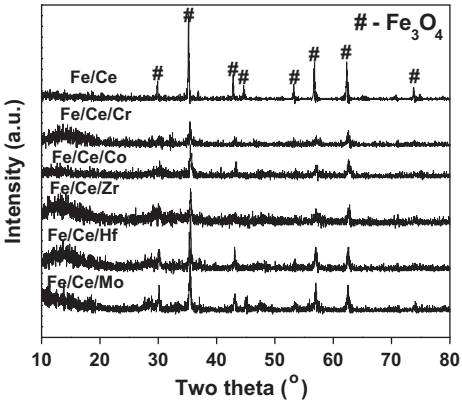

Fig. 6. X-ray powder diffraction patterns of Fe/Ce and various Fe/Ce/M (M = Cr, Co, Zr, Hf, and Mo) spent catalysts (tested at 550 °C) (* – Fe_3O_4, + – CeO_2).

at steam/CO ratio = 1.5 show reflections of magnetite phase only. These data show that our catalysts are quite stable upon WGS reaction. On the whole, XRD results demonstrate that the Fe/Ce and metal doped Fe/Ce fresh calcined catalysts primarily crystallize in the hematite phase and they are converted into the magnetite phase upon activation. The phase retains its structure during the WGS reaction without reducing into either FeO or metallic iron.

The lattice parameter of Fe_3O_4 phase was calculated using interplanar spacing to establish whether metal dopant ions enter into the magnetite lattice upon activation [21]. The lattice parameters of Fe/Ce and metal doped Fe/Ce *activated* and *spent* catalysts after the WGS reaction at steam/CO = 1.5 and in the presence of 400 ppm of H_2S appear in Table 1. Co-, Zr-, Hf-, and Mo-doped Fe/Ce catalysts exhibit lattice expansion, whereas Cr-doped Fe/Ce catalysts exhibit lattice contraction compared to the Fe/Ce catalyst. All dopants except Cr possess a larger ionic radius than Fe^{3+} leading to the lattice (cell volume) expansion. In contrast, Cr^{3+} replaces Fe^{3+} ions at octahedral sites, and the distance between them is reduced, leading to the lattice (cell volume) contraction. A decrease in magnetite lattice spacing is observed for the *spent* Fe/Ce and Co-, Zr-, Hf-, and Mo-doped Fe/Ce catalysts after the WGS reaction at steam/CO ratio = 1.5 and in the presence of sulfur compared to the *activated* catalysts. This is due to the rearrangement of Fe ions between the O_h and T_d sites during the WGS reaction. These results are well agreed with our previous results [9]. Our previous studies also had shown the structural rearrangement of Fe^{2+} and Fe^{3+} ions in both Fe_3O_4 and Fe/Cr (10:0.2) during the WGS reaction and exhibited less WGS activity. On the other hand, Cr-doped Fe/Ce catalyst exhibits no detectable change in the lattice parameter after the WGS reaction. These data suggest that Cr dopant serves to stabilize the magnetite structure during the WGS reaction.

Crystallite sizes of magnetite phase are determined using the Debye–Scheer equation and used to elucidate the role of processing such as activation and WGS reaction on the sintering of the magnetite phase. The crystallite sizes of *as-prepared*, *activated*, *spent* Fe/Ce and metal doped Fe/Ce catalysts after the WGS reaction at a steam/CO ratio = 1.5 and in the presence of 400 ppm of sulfur are presented in Table 2. Due to the amorphous nature of the patterns, it is not possible to determine the crystallite sizes of Cr- and Co-doped Fe/Ce *as-prepared* catalysts. On the other hand, the remaining ferrites, i.e., Fe/Ce and Zr-, Hf-, and Mo-doped Fe/Ce ferrites, were nanocrystalline in *as-prepared* state. Zr, Hf, and Mo, as dopants in Fe/Ce, neither decreased nor increased the crystallite size of hematite in relation to the pristine Fe/Ce catalyst. After activation in a controlled atmosphere, the crystallite sizes of the Fe/Ce and metal doped Fe/Ce catalysts increased [35]. Both Cr- and Co-doped Fe/Ce catalysts exhibited smaller crystallite sizes compared to the pristine Fe/Ce catalyst. Zr-, Hf-, and Mo-doped Fe/Ce catalysts had little or no effect on the sintering of the magnetite phase during activation and exhibited crystallite sizes similar to that of the pristine Fe/Ce. On the other hand, both Cr and Co hindered the sintering of the magnetite phase during the activation. A rapid increase in the crystallite size was observed in the *spent* Fe/Ce catalyst at a steam/CO ratio = 1.5 and in the presence of 400 ppm of sulfur. In the case of both Cr- and Co-doped Fe/Ce catalysts, no evidence of sintering of the magnetite phase was observed upon WGS reaction for 12 h. Other dopants Zr, Hf, and Mo had no or little effect on the sintering of the magnetite phase during the WGS reaction; they exhibited similar crystallite sizes. XRD measurements suggested formation of a solid solution between Ce and Zr/Hf. But it is unable to prevent the sintering of magnetite phase during the activation as well as during the WGS reaction. BET surface area and pore diameter values of Fe/Ce and metal doped Fe/Ce catalysts are presented in Table 1. Both Cr- and Co-doped Fe/Ce catalysts exhibited higher surface areas compared to Fe/Ce, whereas other dopants Zr, Hf, and Mo did not have any influence on the surface area of the Fe/Ce. A narrow particle size distribution of 7.5–10 nm was observed in all cases.

Table 1
BET surface area, pore diameter, and lattice parameter values of the Fe/Ce and various Fe/Ce/M (M = Cr, Co, Zr, Hf, and Mo) catalysts.

Sample	BET surface area (m^2/g)	Pore diameter (nm)	Lattice parameter*	
			Activated	Spent
Fe/Ce	98	81	8.44 ± 0.001	8.37 ± 0.001
Fe/Ce/Cr	150	75	8.39 ± 0.01	8.4 ± 0.01
Fe/Ce/Co	135	78	8.46 ± 0.01	8.4 ± 0.01
Fe/Ce/Zr	100	83	8.48 ± 0.001	8.38 ± 0.001
Fe/Ce/Hf	99	85	8.49 ± 0.001	8.38 ± 0.001
Fe/Ce/Mo	95	98	8.44 ± 0.001	8.37 ± 0.001

* Calculated following standard indexation procedures from the peaks (3 1 1).

Table 2
Crystallite size values of the Fe/Ce and various Fe/Ce/M (M = Cr, Co, Zr, Hf, and Mo) fresh, activated, and spent catalysts after the WGS reaction at steam to CO ratio 1.5.

Sample	Crystallite size[a]		
	Fresh	Activated	Used*
Fe/Ce	9	15	23
Fe/Ce/Cr	nd	6	6.8
Fe/Ce/Co	nd	7.1	8.2
Fe/Ce/Zr	6.5	11	20
Fe/Ce/Hf	6	9	22.5
Fe/Ce/Mo	10	16	22

nd: Not determined due to amorphous nature.
[a] Calculated using Debye–Scheer equation The error in crystallite size is ±0.1.
* Samples activated at 400 °C in the presence of process gas and tested at 550 °C.

3.2. TPR measurements

Temperature-programmed reduction measurements were performed over Fe/Ce and metal doped Fe/Ce catalysts to examine the effect of foreign metal on the reducibility of hematite and ceria. The temperature maxima of each transition for various catalysts are presented in Table 3. As reported in our previous studies [36], Fe/Ce catalyst exhibits total four peaks in its TPR profile. These peaks primarily belong to surface ceria reduction, hematite to magnetite transition, magnetite to wustite transition, and wustite to metallic iron transitions, respectively. In Fe/Ce, the hematite to magnetite transition occurred at 300 °C, and surface ceria reduction occurred at 330 °C. The magnetite to wustite reduction occurred at 566 °C. Cr-doped Fe/Ce catalyst exhibited surface ceria reduction peak at 333 °C, hematite to magnetite reduction at 305 °C, and magnetite to wustite transition at 566 °C. Similarly, Co-doped Fe/Ce catalyst also exhibited surface ceria, hematite to magnetite, and magnetite to wustite transitions at 315 °C, 310 °C, and 550 °C, respectively. These results suggest that doping of Cr/Co-doping into Fe/Ce did not have any effect on the reducibility of surface ceria, hematite to magnetite transition, or magnetite to wustite transitions. In case of Cr-, Co-, and Mo-doped Fe/Ce

Table 3
T_{max} (°C) values of various phase transformations of the Fe/Ce and various Fe/Ce/M.

Sample	Fe_2O_3 to Fe_3O_4	Fe_3O_4 to FeO	Surface ceria
Fe/Ce	300	566	328
Fe/Ce/Cr	303	566	310
Fe/Ce/Co	306	550	315
Fe/Ce/Zr	290	528	230
Fe/Ce/Hf	308	521	239
Fe/Ce/Mo	302	595	318

(M = Cr, Co, Zr, Hf, and Mo) catalysts.

catalysts, hematite to magnetite reduction occurred earlier than surface ceria reduction, whereas in case of Zr, Hf doped catalysts, they occurred in opposite way. This is due to the formation of solid solutions between Ce and Zr/Hf as revealed by XRD measurements. But there is no change in the reduction temperature of either hematite to magnetite or magnetite to wustite transitions. Hence, formation of solid solution between Ce and Zr/Hf did not have any effect on the reducibility of hematite to magnetite transition. Like Cr and Co, doping Fe/Ce with Mo did not show any effect on the reducibility of surface ceria or $Fe_2O_3 \rightarrow Fe_3O_4 \rightarrow FeO$ transitions. On the whole, our TPR results show that any of the doped metal exhibits neither promotional effect nor inhibition effect on the transition temperature of $Fe_2O_3 \rightarrow Fe_3O_4 \rightarrow FeO$ transformations.

3.3. Mössbauer spectroscopic measurements

X-ray diffraction is necessary but not a sufficient technique for the structural characterization of powders of the $Fe_{3-x}O_4$ system. Mössbauer spectroscopy is a particularly powerful probe to elucidate the Fe local structure and to understand the role of dopant on stoichiometry in the present catalysts. The *as-prepared*, *activated*, and *spent* Fe/Ce and metal doped Fe/Ce catalysts after WGS reaction at steam/CO ratio = 1.5 and in the presence of sulfur were therefore further characterized by using Mössbauer spectroscopy at room temperature. These data provide invaluable insights into the relative proportions of Fe^{2+} and Fe^{3+} in different local structures and oxygen coordination. XRD results suggest that all the catalysts contain hematite phase in *as-prepared* catalysts and magnetite phase in *activated* and *spent* catalysts. At room temperature, hematite exhibits one 6 line pattern due to Fe^{3+} ions at octahedral sites in Mössbauer spectroscopy [9]. On the other hand, magnetite exhibits two six line patterns; one pattern arises from Fe^{3+} ions at tetrahedral sites, while the other from contributions of both Fe^{3+} and Fe^{2+} ions at octahedral sites [37]. The Mössbauer spectra of pure magnetite and Fe/Cr catalysts were reported in our earlier publication [35]. The Mössbauer spectra of *as-prepared*, *activated,* and *spent* Fe/Ce and the Cr-, Co-, and Zr-doped Fe/Ce catalysts are presented, respectively, in Figs. 7–10. The isomer shift (δ), magnetic field (H), and quadruple splitting (Δ) values deduced from these data are presented in Table 4. The fraction of super-paramagnetic phase formed in these catalysts values is shown in Table 5. As reported in previous studies, the *as-prepared* Fe/Ce before activation exhibits one six line pattern and a peak at zero velocity [9]. The six line pattern arises from the Fe^{3+} ions at octahedral sites of Hematite. The peak near zero velocity is attributed to super -paramagnetic phase formed in the catalyst. Super-paramagnetism arises from Fe_3O_4 particles of <5 nm crystallite size. Fe/Ce catalyst exhibits a 49% of super-paramagnetic fraction in the *as-prepared* state. The *activated* and *spent* Fe/Ce catalyst exhibits two six line patterns in the Mössbauer spectra (Fig. 7b and c). The pattern with higher magnetic field arises from the Fe^{3+} ions at tetrahedral sites while that pattern with the lower magnetic field from the Fe^{3+} and Fe^{2+} ions at the octahedral sites. The δ, H, and Δ values presented in Table 4 agree well with earlier reports [38]. Interestingly, the fraction of super-paramagnetic phase decreased from 49 to 18% after activating the Fe/Ce catalyst, and it disappeared completely after the WGS reaction at steam/CO ratio = 1.5 and in the presence of sulfur. These results agree well with crystallite size considerations, viz., an increase due to the sintering of the magnetite phase upon activation and WGS reaction in the Fe/Ce catalyst. On the other hand, Cr-doped Fe/Ce catalyst (Fig. 8) exhibited 95% of super-paramagnetic phase in the *as-prepared* state, about 80% in the *activated*, and 70% *spent* state. These results suggest that the

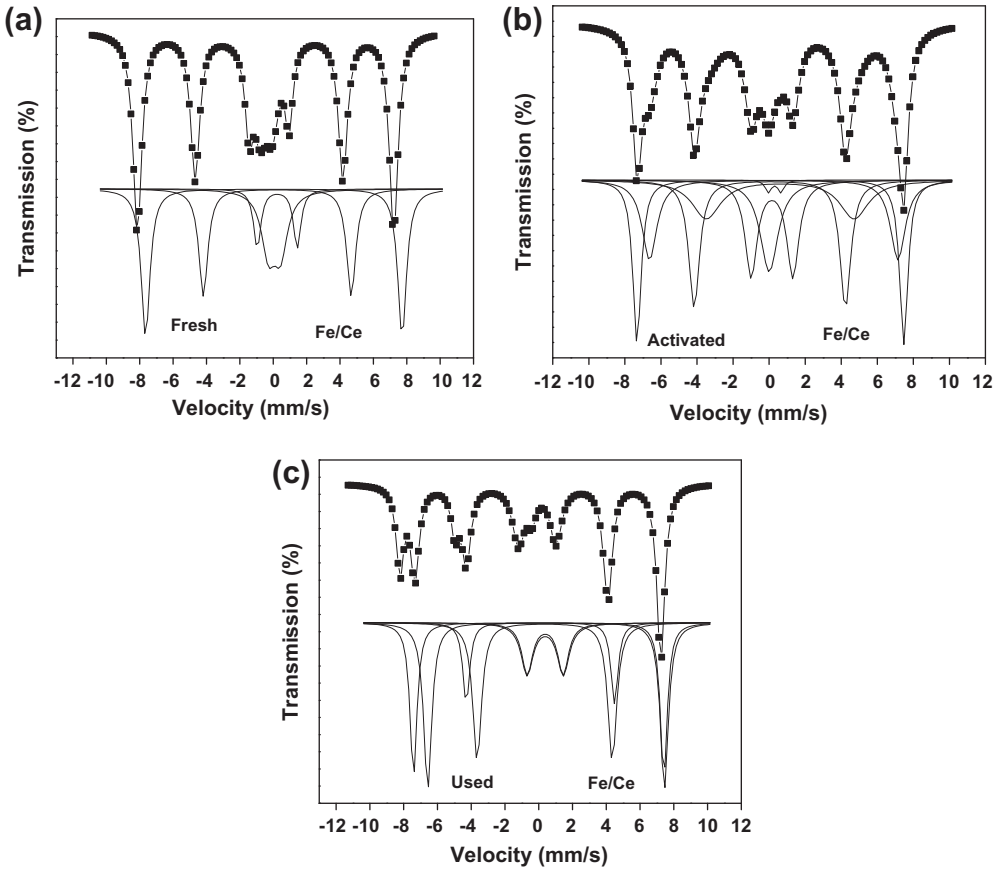

Fig. 7. Mossbauer spectra of Fe/Ce catalysts: (a) fresh, (b) activated, and (c) spent.

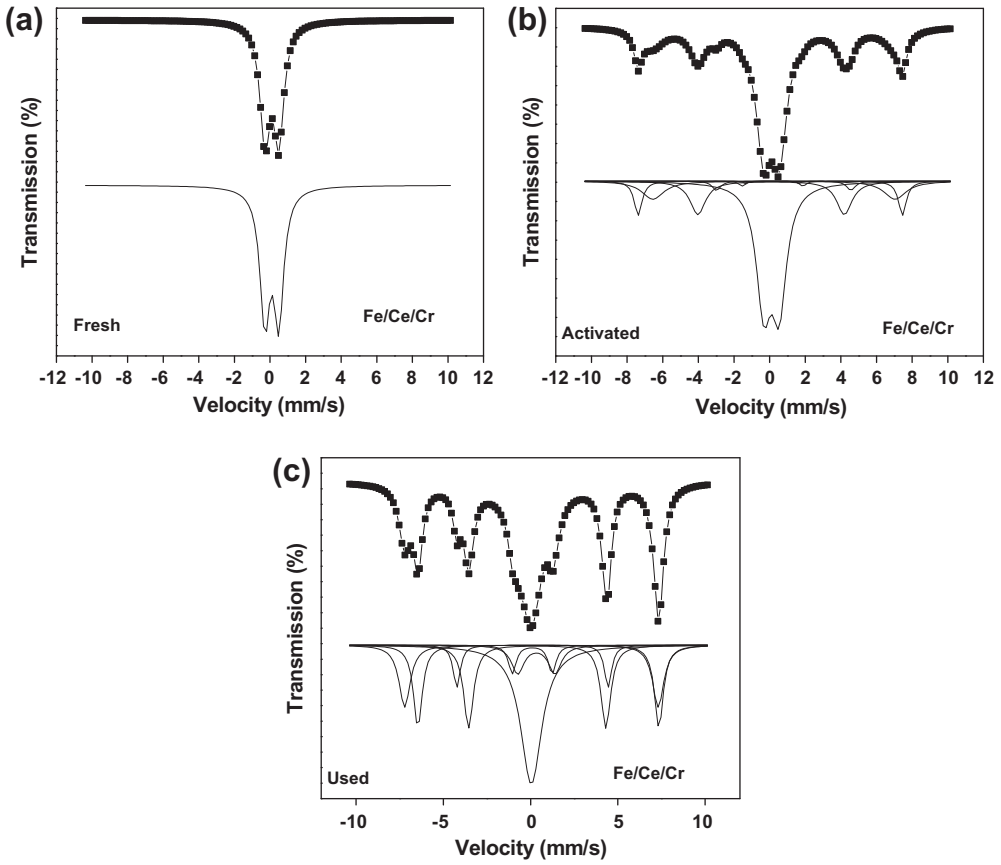

Fig. 8. Mossbauer spectra of Fe/Ce/Cr catalysts: (a) fresh, (b) activated, and (c) spent.

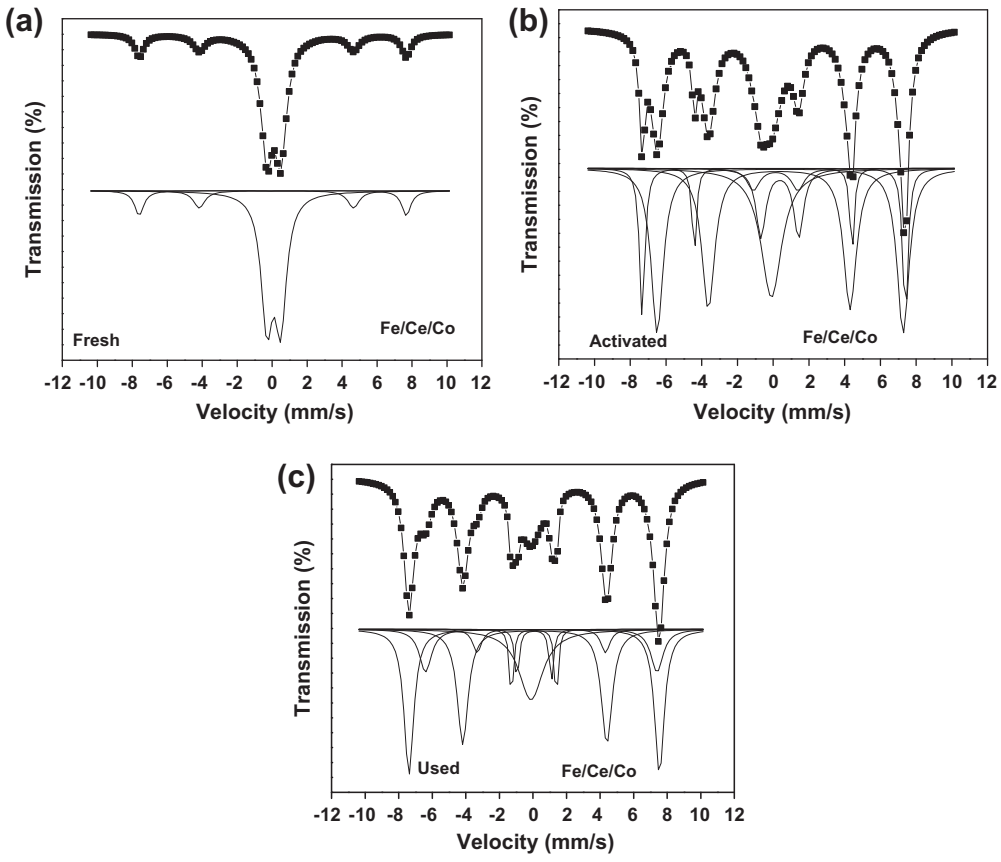

Fig. 9. Mossbauer spectra of Fe/Ce/Co catalysts: (a) fresh, (b) activated, and (c) spent.

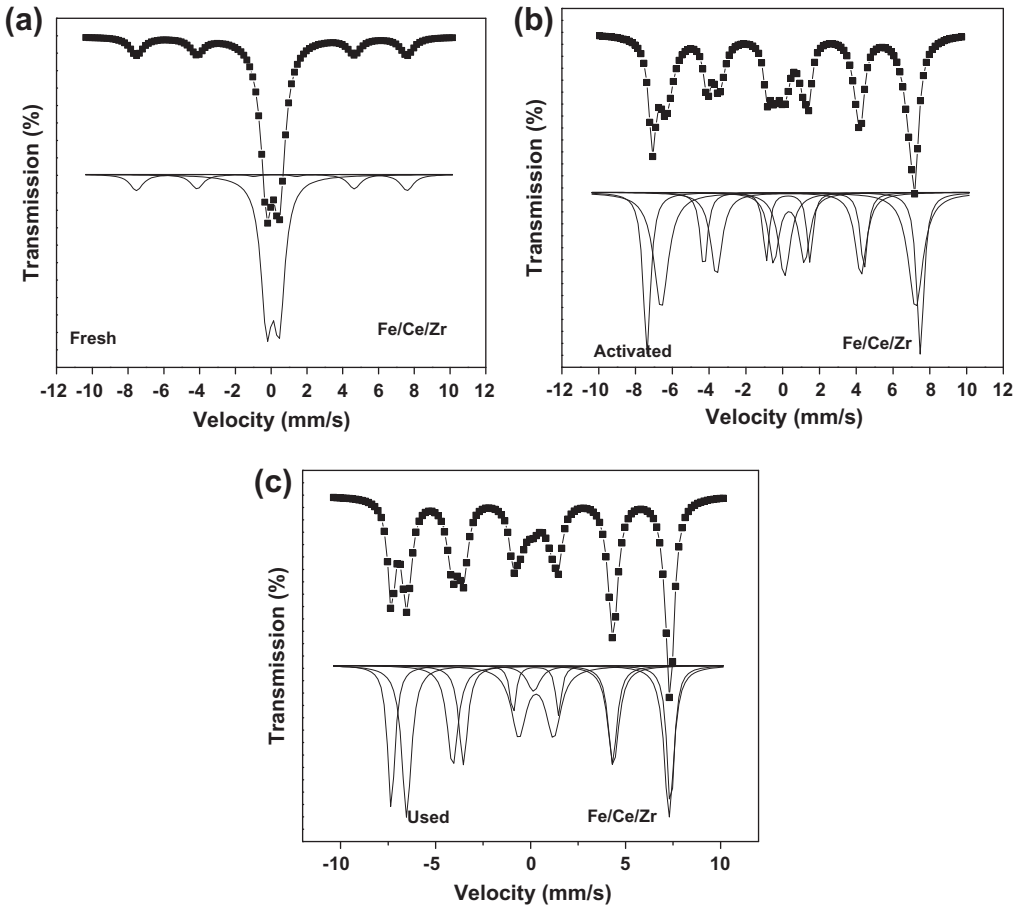

Fig. 10. Mossbauer spectra of Fe/Ce/Zr catalysts: (a) fresh, (b) activated, and (c) spent.

Table 4
Isomer shift (δ), magnetic field (H), and quadrapole splitting (Δ) various Fe/Ce/M (M = Cr, Co, Zr, Hf, and Mo) catalysts. Isomer shifts are quoted relative to α-Fe at room temperature.

Sample	Tetrahedral sites			Octahedral sites		
	δ^a (mm/s)	kOe(T)	Δ (mm/s)	δ^a (mm/s)	kOe(T)	Δ (mm/s)
Fe/Ce	0.25	492	−0.01	0.43	458	0.18
Fe/Ce (spent)	0.25	493	0.04	0.42	466	−0.03
Fe/Ce/Cr	0.25	493	0.02	0.36	452	0.27
Fe/Ce/Cr (spent)	0.26	483	0.02	0.35	459	−0.03
Fe/Ce/Co	0.25	499	0.01	0.38	473	−0.01
Fe/Ce/Co (spent)	0.26	490	0.05	0.39	460	0.01
Fe/Ce/Zr	0.26	496	0.02	0.43	460	−0.02
Fe/Ce/Zr (spent)	0.25	495	0.01	0.41	460	0.01
Fe/Ce/Hf	0.27	488	0.06	0.42	455	0.02
Fe/Ce/Hf (spent)	0.25	490	−0.02	0.42	458	−0.02
Fe/Ce/Mo	0.26	495	0.02	0.43	460	−0.01
Fe/Ce/Mo (spent)	0.26	486	0.04	0.42	457	0.07

The error in δ is ±0.02 mm/s, in Δ is ±0.02 mm/s, and in H is ±5 koe.

Table 5
Super-paramagnetic fraction in Fe/Ce and various Fe/Ce/M (M = Cr, Co, Zr, Hf, and Mo) catalysts.

Sample	Fraction of super-paramagnetic Nature (%)		
	Fresh	Activated	Used
Fe/Ce	49	18	0
Fe/Ce/Cr	95	80	70
Fe/Ce/Co	88	50	48
Fe/Ce/Zr	78	20	2
Fe/Ce/Hf	70	10	1.5
Fe/Ce/Mo	44	14	0

The error in fraction of super-paramagnetic nature is ±7.

Cr-doped catalyst contains 70% of the Fe_3O_4 phase nanoparticles even after the WGS reaction. This nanophase, most likely, is responsible for the higher WGS activity. We note that the δ and H values at T_d sites of *Cr-activated* catalyst (Table 4) are similar to those of the *activated* Fe/Ce catalyst. On the other hand, both δ and H values for O_h sites in the *Cr-activated* catalyst decreased when compared to the *activated* Fe/Ce catalyst (no Cr-doping). These results show that Cr selectively enters at the octahedral sites of the magnetite upon activation to replace equal amounts of Fe^{3+} and Fe^{2+} ions as reported [39]. Co-doping in analogy to Cr-doping (Fig. 9) also leads to a reduction in δ and H values at O_h sites compared to the Fe/Ce catalyst but to a lesser degree. Here also, *Co-doping* retains 48% of super-paramagnetic phase after WGS reaction at steam/CO ratio = 1.5 and in the presence of sulfur. On the other hand, Mössbauer spectra of *as-prepared*, *activated*, and *spent* Zr- (Fig. 10), Hf- (not shown), and Mo (not shown)-doped Fe/Ce catalysts are similar to those of Fe/Ce catalyst. The δ and H values at both octahedral (O_h) and tetrahedral (T_d) sites after activation and after the WGS reaction in these metal doped catalysts are similar to the δ and H values of the Fe/Ce catalyst. The super-paramagnetic phases of these metal doped catalysts also decrease after activation

and the fraction vanished completely after the WGS reaction. In Mössbauer spectroscopy, super-paramagnetism usually leads to a collapse of the hyperfine structure into a doublet feature near $v = 0$ mm/s. In some of the catalysts, we observed such a doublet. To check whether this doublet is due to super-paramagnetism component or simply due to a quadruple doublet, we performed measurements at 78 K and found the doublet feature to exhibit Zeeman splitting. These results suggest that the doublet is due to the super-paramagnetic component. On the whole, Mössbauer spectroscopic measurements show that both Cr- and Co-dopants preferentially replace iron ions at octahedral sites in magnetite phase during activation and promote WGS activity. On the other hand, Zr, Hf, and Mo apparently have no or little effect either the structure or catalytic properties of magnetite upon activation and upon WGS reaction.

3.4. XPS measurements

To verify the elemental oxidation states and to investigate changes to surface structure upon activation and WGS reaction, X-ray photoelectron spectroscopy (XPS) measurements were performed on *activated* and *spent* catalysts after the WGS reaction at steam/CO ratio = 1.5 and in the presence of sulfur. The photoelectron peaks of O 1s, Fe 2p, Ce 3d of the *activated* and *spent* catalysts after the WGS reaction are presented in Figs. 11–13Figs. 11. The corresponding electron binding energies of O 1s, Ce 3d, Fe 2p photoelectron peaks are shown in Table 6. The O 1s spectra of *activated* Fe/Ce and metal doped Fe/Ce catalysts are broad and complicated (Fig. 11a) due to overlapping contribution from iron and ceria in Fe/Ce and iron, ceria, and other metal dopants in the case of metal

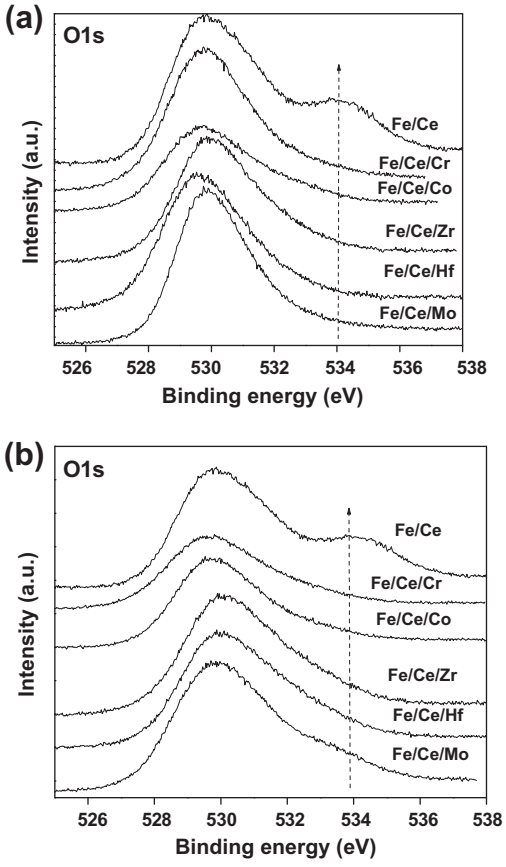

Fig. 11. O1s XPS spectra of Fe/Ce and various Fe/Ce/M (M = Cr, Co, Zr, Hf, and Mo) catalysts: (a) activated catalysts and (b) spent catalysts.

Table 6
XPS core level binding energies of Fe/Ce and various Fe/Ce/M (M = Cr, Co, Zr, Hf, and Mo) catalysts.

Sample	O1s	Fe 2p	Ce 3d	Surface Fe^{3+}/Fe^{2+} ratio	% of U^{III} peak of Ce 3d
Fe/Ce	529.8	712.4		1.8 ± 0.1	10.96
Fe/Ce (spent)	529.7	711		1 ± 0.1	10.6
Fe/Ce/Cr	529.7	712		1.98 ± 0.1	4.82
Fe/Ce/Cr (spent)	529.6	711.1		2.18 ± 0.1	5
Fe/Ce/Co	529.7	711.9		1.9 ± 0.1	8
Fe/Ce/Co (spent)	529.7	711		2.1 ± 0.1	8.1
Fe/Ce/Zr	529.8	711.2		2.47 ± 0.1	9.31
Fe/Ce/Zr (spent)	530	712		2.15 ± 0.1	8.27
Fe/Ce/Hf	529.7	712.4		2.54 ± 0.1	8.7
Fe/Ce/Hf (spent)	530	711.4		1.89 ± 0.1	8.3
Fe/Ce/Mo	529.5	711.6		2.63 ± 0.1	10.9
Fe/Ce/Mo (spent)	529.9	710.8		1.13 ± 0.1	10.2

doped Fe/Ce catalysts [40]. The O 1s binding energies of Fe_3O_4 and CeO_2 are 529.7 and 530.2 eV, respectively [41]. The binding energy of most intense peak in the case of Fe/Ce is observed at 529.8, and it comes from oxygen atoms that are bound to Fe [42], as suggested by electronegativity coordinations as well. An additional peak at 534 eV in Fe/Ce catalyst is identified with formation of carbonate species in the activation process. Recall that during the activation, we used process gas which is a mixture of CO, CO_2, H_2, and steam to convert hematite into active magnetite. Carbonate formation occurs via reaction of either CO or CO_2. Upon Cr-, Co-, Zr-, Hf-, and Mo-doping, there is not much change in the O1s binding energy of Fe/Ce catalysts, which indicates that oxygen species on the surface of the metal doped Fe/Ce catalyst mostly bond to Fe. Interestingly, the peak due to the carbonate formation is not observed in any of the metal doped Fe/Ce activated catalysts, clearly showing that metal dopants in Fe/Ce catalyst preclude carbonate formation during activation. The O1s spectra of Fe/Ce and metal doped Fe/Ce *spent* catalysts after the WGS reaction are presented in Fig. 11b. As represented in Fig. 11b and Table 6, the Fe/Ce spent catalyst after the WGS reaction exhibits an intense peak at 529.7 with a satellite at 534 eV in the O 1s spectra. The peak at 529.7 is due to the oxygen atoms bounded to the iron, and the satellite is due to the formation of carbonate species. All the metal doped Fe/Ce catalysts also exhibit a peak at around 529.7 which conforms that after the WGS reaction also, most of the surface was occupied by iron species. Cr- and Co-doped catalysts did not exhibit any peak due to carbonate formation at 534 after the WGS reaction; on the other hand, Zr-, Hf-, and Mo-doped catalysts exhibit a less intense peak at 534 due to the carbonate formation. These results confirm that both Cr and Co prevent the magnetite from the carbonate formation during the activation and the WGS reaction, whereas Zr, Hf, and Mo able to prevent the magnetite only during the activation but not during the WGS reaction.

Fe 2p XPS spectra of Fe/Ce and various metal doped Fe/Ce *activated* catalysts typically show peaks (see Table 6, Fig. 12) due to magnetite with contributions from both Fe^{2+} and Fe^{3+}. Specifically, peaks in the region 709–713 eV with a satellite around 725 eV come from ionization from Fe $2p_{3/2}$ and Fe $2p_{1/2}$ states in magnetite, respectively [43]. Fe^{2+} exhibits peaks around 709–711 eV with a satellite around 723 eV, while Fe^{3+} exhibits a peak around 712–713 eV with a satellite at 725–727 eV [43]. By deconvoluting, the observed line shape as an appropriate super position of Gaussian profiles of Fe^{2+}/Fe^{3+} ratio on the surface of the magnetite phase was established. The ratios for Fe/Ce and various metal doped Fe/Ce catalysts are reproduced in Table 6. In magnetite, 2/3 sites are occupied by Fe^{3+} ions and 1/3 sites by Fe^{2+} ions leading to a Fe^{2+}/Fe^{3+} ratio in the bulk. XPS results show that during the activation, neither Ce nor a third metal dopant caused any surface structural rearrangement of Fe^{3+} and Fe^{2+} ions. Fe2p XPS measurements were

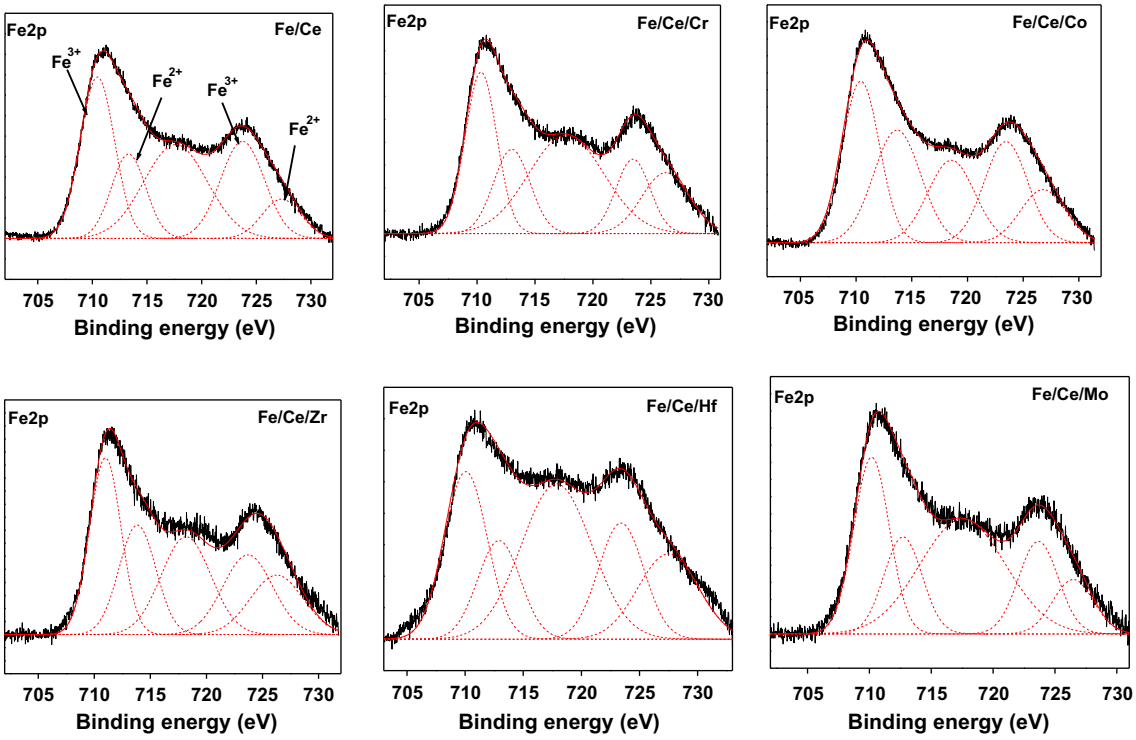

Fig. 12. Fe2p XPS spectra of Fe/Ce and various Fe/Ce/M (M = Cr, Co, Zr, Hf, and Mo) activated catalysts.

also performed over *spent* catalysts after the WGS reaction at steam to CO ratio of 1.5 and in the presence of sulfur. Similar XPS profiles were observed for the *spent* catalysts after the WGS reaction. It should be noted that all catalysts exhibited peaks due to only magnetite but with different surface Fe^{3+}/Fe^{2+} ratios. After the WGS reaction, both Cr- and Co-doped Fe/Ce catalysts exhibited a surface Fe^{3+}/Fe^{2+} ratios close to 2, which is similar to the activated catalysts. On the other hand, Fe/Ce and Zr-, Hf-, and Mo-doped Fe/Ce catalysts exhibited lesser surface Fe^{3+}/Fe^{2+} ratios compared to the corresponding activated catalysts. This is due to the structural rearrangement of Fe^{3+} and Fe^{2+} ions during the WGS reaction. Thus, XPS data show that both Cr and Co stabilize the magnetite during the WGS reaction.

Typically, the Ce 3d XPS core level spectra exhibit three lobed envelopes (around 879–890, 895–910, and 916 eV) such as those depicted in Fig. 13 for Fe/Ce and metal doped Fe/Ce *activated* catalysts, respectively. From these envelopes, the coexistence of both Ce^{3+} and Ce^{4+} oxidation states is distinguishable, although the 4+ oxidation state is predominant. Because of the complex shape of the spectrum for nonstoichiometric cerium oxide, it is postulated that the Ce 3d spectrum arises from the partially oxidized surface Ce species in the catalysts and can be approximated as a linear combination of the spectra characterizing the stoichiometric oxides with 3+ and 4+ valence states [44]. Further, it can be individually resolved into four sets of features grouped as u and v lines, respectively, to denote the electronic transitions in the $3d_{3/2}$ and $3d_{5/2}$ levels, following the notation of Burroughs et al., the peaks labeled v and v^{I} have been assigned to a mixing of Ce $3d^9$ $4f^2$ O $2p^4$ and Ce $3d^9$ $4f^1$ O $2p^5$ Ce(IV) final states, and the peak denoted as v^{III} corresponds to the Ce $3d^9$ 4f0 O 2p6 Ce(IV) final state [45]. On the other hand, line v^{I} is assigned to the Ce $3d^9$ $4f^0$ O $2p^6$ Ce (III) final states. The same assignment can be applied to the u structures, which correspond to the Ce $3d^{3/2}$ levels. As represented in Fig. 13, the Fe/Ce and metal doped Fe/Ce catalysts exhibit peaks due to both the Ce^{4+} and Ce^{3+} oxidation states. Generally, the Ce^{3+} content is determined by calculating the area under the peaks u' and v'. However, the v' line always occurs along with the v'' contribution and so can difficult to find out the area. The same phenomena will be applied to u', and it occurs along with u. Therefore, the % of area of u''' peak to the total area is used to determine the surface concentration of Ce^{3+} in the mixed oxide in the literature. In pure ceria, percentage of the $u(''')$ peak is 14 [46]. As represented in table 4, the percentage of the $u(''')$ peak is 10.96 for the Fe/Ce catalyst after the activation. All the metal doped Fe/Ce catalysts exhibit lesser values of percentage of the $u(''')$ peak compared to the Fe/Ce catalysts except Fe/Ce/Mo. The amount of Ce^{3+} in various metal doped Fe/Ce catalysts follows the order Fe/Ce/Cr > Fe/Ce/Co > Fe/Ce/Hf > Fe/Ce/Zr > Fe/Ce/Mo. Mossbauer spectroscopic results revealed that both Cr and Co entered at octahedral sites of the magnetite lattice along with the cerium during the activation. During this process, some of the Ce^{4+} will be reduced to Ce^{3+}. This could be the reason why both Cr- and Co-doped Fe/Ce catalysts contain higher amount of Ce^{3+}. The observed higher amount of Ce^{3+} in both Fe/Ce/Zr and Fe/Ce/Hf catalysts is due to the formation of solid solution between Ce and Zr/Hf in accordance with XRD and TPR results. On the other hand, Mo-doped contains same amount of Ce^{3+} as Fe/Ce, which conforms that Mo has no effect on the structure of Fe/Ce catalyst which corroborating with other characterization results. As represented in Table 6, there is not much change in the amount of Ce^{3+} of the Fe/Ce and metal doped Fe/Ce catalysts after WGS reaction.

3.5. Structure–activity relationship

Simultaneous precipitation of metal nitrates along with iron and cerium nitrates leads to the formation of high surface area $Fe_{1.6}Ce_{0.2}M_{0.2}$ (M = Cr, Co, Zr, Hf, and Mo) type of spinels. After activation in a controlled atmosphere, these spinels converted into either mixed or inverse spinels. All the catalysts exhibited equilibrium conversions at steam to ratio 3.5. Among the various dopants, Cr- and Co-doped Fe/Ce catalysts exhibited equilibrium conversions even at steam/CO ratio = 1.5. When we plot normalized CO

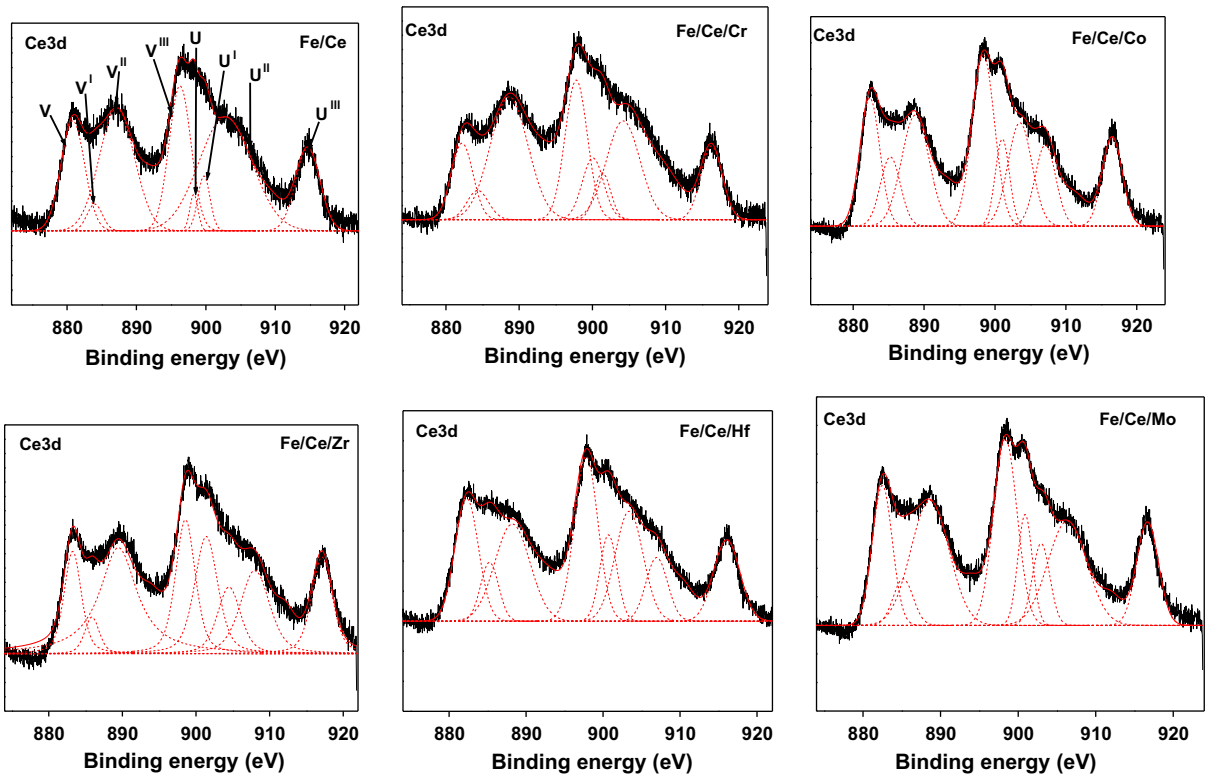

Fig. 13. Ce 3d XPS spectra of Fe/Ce and various Fe/Ce/M (M = Cr, Co, Zr, Hf, and Mo) activated catalysts.

conversion per unit surface area, both Co- and Cr-doped Fe/Ce catalysts exhibited higher activity. These results suggest that the higher activity of Cr- and Co-doped Fe/Ce catalysts is due to both higher surface area and promotional effect of Cr and Co. We observed that there is no decrease in WGS activity in any of the catalyst in the presence of 400 ppm of sulfur. There is not much change in the BET surface and pore diameter of Fe/Ce catalyst upon metal doping. Mössbauer effect and lattice parameters suggest that both Cr and Co dopants enter at octahedral sites in magnetite and exhibit higher super-paramagnetic fraction even after the WGS reaction. O 1s spectra results indicate that both Cr and Co dopants prevent magnetite to carbonate formation during activation as well as during WGS reaction. Other metal dopants, Zr, Hf, and Mo, also inhibit carbonate formation during activation, but carbonate formation is observed upon WGS reaction. Fe 2p XPS results suggest that there is a structural rearrangement of Fe^{2+} and Fe^{3+} on the surface of magnetite during the WGS reaction in case of Fe/Ce and Zr-, Hf-, and Mo-doped Fe/Ce catalyst. No such rearrangement appears in the case of Cr- and Co-doped Fe/Ce catalysts. On the whole, both Cr and Co dopants selectively replace octahedral sites of magnetite lattice during activation and prevent the magnetite phase from sintering as well as structural rearrangements during the WGS reaction to exhibit high WGS activity. Even though there is a solid solution formation between Ce and Zr/Hf, these dopants do not facilitate sintering of magnetite during the WGS reaction.

4. Conclusions

High surface area $Fe_{1.6}Ce_{0.2}M_{0.2}O_3$ (M = Cr, Co, Zr, Hf, and Mo) type of spinels was synthesised by ammonia assisted co-precipitation method. After activation in the presence of process gas, these spinels converted into mixed or inverse spinels. High temperature WGS reaction was performed over the activated spinels at steam/CO ratios of 3.5 and 1.5 in the 400 °C < T < 550 °C. Both Cr- and Co-doped Fe/Ce catalysts exhibited excellent WGS activity even at steam/CO ratio = 1.5. We observed no decrease in the activity for all the catalysts tested in the presence of 400 ppm of sulfur. XRD and lattice parameter results suggest the substitution of dopant into the magnetite cubic lattice during the activation. TPR results indicate that the dopants (Cr and Co) have no effect on either the reducibility of hematite to magnetite, or of magnetite to wustite. Addition of Zr and Hf to Fe/Ce lowers the reduction temperature of surface ceria due to the formation of solid solutions. Fe 2p XPS results establish that both Cr and Co inhibit the structural rearrangement of Fe^{2+} and Fe^{3+} on the surface of magnetite during the WGS reaction. Mössbauer spectroscopy studies show local structural distortions in the magnetite phase as the lattice contracts or expands. These distortions are observed from changes in the internal magnetic field and isomer shift at octahedral Fe sites upon Cr- and Co-doping in Fe/Ce catalysts. Mössbauer spectroscopy also shows that both Cr and Co are able to retain their super-paramagnetic fraction after the WGS reaction. Our results show that both Cr and Co substitute at octahedral sites in magnetite during the activation and prevent the magnetite phase from sintering, and promoting the WGS activity of Fe/Ce. Other dopants such as Zr, Hf, and Mo have little or no effect on either the crystallographic structure or catalytic activity of Fe/Ce.

Acknowledgments

Financial support was provided by the US Department of Energy (Grant DE-PS36-03GO93007). The authors also thank OCDO for providing some of the financial support.

References

[1] E. Kikuchi, S. Uemiya, N. Sato, H. Inoue, T. Matsuda, Chem. Lett. (1989) 489.
[2] S. Uemiya, N. Sato, H. Ando, E. Kikuchi, Ind. Eng. Chem. Res. 30 (1991) 585.

[3] A. Basile, E. Drioli, F. Santella, V. Violante, G. Capannelli, G. Vitulli, Gas. Sep. Purif. 10 (1996) 53.
[4] A. Basile, A. Crscuoli, F. Santella, E. Drioli, Gas. Sep. Purif. 10 (1996) 243.
[5] A. Criscuoli, A. Basile, E. Drioli, O. Loiacono, J. Membrane Sci. 181 (2001) 21.
[6] A. Criscuoli, A. Basile, E. Drioli, Catal. Today 56 (2000) 53.
[7] A. Basile, G. Chiappetta, S. Tosti, V. Violante, Sep. Purif. Technol. 25 (2001) 549.
[8] A. Brunetti, A. Caravella, G. Barbieri, E. Drioli, J. Membrane Sci. 306 (2007) 329.
[9] A. Khan, P. Chen, P. Boolchand, P.G. Simrnitios, J. Catal. 253 (2008) 91.
[10] Z. Tang, S.J. Kim, G.K. Reddy, J. Dong, P. Smirniotis, J. Membrane Sci. 354 (2010) 114.
[11] A. Trovarelli (Ed.), Catalysis by Ceria and Related Materials, World Scientific, London, 2002.
[12] V.E. Henrich, P.A. Cox, The Surface Science of Metal Oxides, Cambridge University Press, Cambridge, UK, 1994.
[13] M. Fernádez-García, A. Martínez-Arias, J.C. Hanson, J.A. Rodriguez, Chem. Rev. 104 (2004) 4063.
[14] R.W. Wyckoff, Crystal Structures, second ed., Wiley, New York, 1964.
[15] W.C. Mackrodt, M. Fowles, M.A. Morris, European Patent 165, 1991, p. 91.
[16] C. Zerva, C.J. Philippopoulos, Appl. Catal. B: Environ. 67 (2006) 105.
[17] F.J.P. Alonso, I.M. Cabrera, M.L. Granados, F. Kapteijn, J.L.G. Fierro, J. Catal. 239 (2006) 340.
[18] G.C. Araujo, M.C. Rangel, Catal. Today 62 (2000) 201.
[19] H.P. Klug, L.E. Alexander, X-ray Diffraction Procedures for Polycrystalline and Amorphous Materials, second ed., Wiley, New York, 1974.
[20] R.D. Shannon, Acta Crystallogr. A 32 (1976) 751.
[21] A.D. Krawitz, Introduction to Diffraction in Materials Science and Engineering, Wiley-Interscience, New York, 2001.
[22] P. Boolchand, S. Pradhan, Y. Wu, M. Abdelgadir, W. Huff, D. Forell, R. Coussement, D. McDaniel, Phys. Rev. B 45 (1992) 921.
[23] C. Rhodes, G.J. Hutchings, A.M. Ward, Catal. Today 23 (1995) 43.
[24] C. Rhodes, B.P. Williams, F. King, G.J. Hutchings, Catal. Commun. 3 (2002) 381.
[25] E. Xue, M. O'Keeffe, J.R.H. Ross, Catal. Today 30 (1996) 107.
[26] I.L. Júnior, J.M.M. Millet, M. Aouine, M.C. Rangel, Appl. Catal. A: Gen. 283 (2005) 91.
[27] L. Lloyd, D.E. Ridler, M.V. Twigg, in: M.V. Twigg (Ed.), Catalyst Handbook, second ed., Wolfe Publishing Ltd., London, 1989, pp. 283–339.
[28] A.L.C. Pereira, G.J.P. Berrocal, S.G. Marchetti, A. Albornoz, A.O. de Souza, M.C. Rangel, J. Mol. Catal.: Gen. 281 (2008) 66.
[29] G.K. Reddy, K. Gunasekara, P. Boolchand, P. Smirniotis, J. Phys. Chem. C 115 (2011) 7586.
[30] D.S. Newsome, Catal. Rev. Sci. Eng. 21 (1980) 275.
[31] S.S. Hla, G.J. Duffy, L.D. Morpeth, A. Cousins, D.G. Roberts, J.H. Edwards, Catal. Commun. 10 (2009) 967.
[32] I.S. Lyubutin, C.R. Lin, V. Korzhetskiy, T.V. Dmitrieva, R.K. Chiang, J. Appl. Phys. 106 (2009) 034311.
[33] B.M. Reddy, K.N. Rao, G.K. Reddy, A. Khan, J. Phys. Chem. C 111 (2007) 18751.
[34] B.M. Reddy, G.K. Reddy, I. Ganesh, J.M.F. Ferriera, J. Mater. Sci. 44 (2009) 2743.
[35] G.K. Reddy, K. Gunasekara, P. Boolchand, P. Smirniotis, J. Phys. Chem. C 115 (2011) 920.
[36] A. Khan, P. Smirniotis, J. Mol. Catal. A: Chem. 280 (2008) 43.
[37] G.K. Reddy, P. Smirniotis, Catal. Lett. 141 (2011) 27.
[38] A.G. Roca, J.F. Marco, M.P. Morales, C.J. Serna, J. Phys. Chem. C 111 (2007) 18577.
[39] H. Topsoe, J.A. Dumesic, M. Boudart, J. Catal. 28 (1973) 477.
[40] G.A. Sawatzky, D. Post, Phys. Rev. B 20 (1979) 1546.
[41] C.D. Wagner, W.M. Riggs, L.E. Davis, J.F. Moulder, in: G.E. Muilenberg (Ed.), Handbook of X-ray Photoelectron Spectroscopy, Perkin-Elmer Corp., CITY, MN, 1978.
[42] I. Imamura, S. Ishida, H. Taramoto, Y. Saito, J. Chem. Soc. Faraday Trans. 89 (1993) 757.
[43] A.L.C. Pereira, G.J.P. Berrocal, S.G. Marchetti, A.A. Alexilda, O. de Souza, M.C. Rangel, J. Mol. Catal. A: Chem. 281 (2008) 66.
[44] J. Stubenrauch, J.M. Vohs, J. Catal. 159 (1996) 50.
[45] A. Burroughs, A. Hamnett, A.F. Orchard, G. Thornton, J. Chem. Soc. Dalton Trans. 1 (1976) 1686.
[46] A. Martnez-Arias, M. Fernandez-Garca, V. Ballesteros, L.N. Salamanca, J.C. Conesa, C. Otero, J. Soria, Langmuir 15 (1999) 4796.